NANO LETTERS

pubs.acs.org/NanoLett Letter

Enhanced Multiphoton Processes in Perovskite Metasurfaces

Yubin Fan,[#] Pavel Tonkaev,[#] Yuhan Wang,[#] Qinghai Song,[*] Jiecai Han, Sergey V. Makarov,[*] Yuri Kivshar,[*] and Shumin Xiao[*]

Cite This: *Nano Lett.* 2021, 21, 7191−7197 Read Online

ACCESS | Metrics & More | Article Recommendations | Supporting Information

ABSTRACT: Multiphoton absorption and luminescence are fundamentally important nonlinear processes for utilizing efficient light−matter interaction. Resonant enhancement of nonlinear processes has been demonstrated for many nanostructures; however, it is believed that all higher-order processes are always much weaker than their corresponding linear processes. Here, we study multiphoton luminescence from structured surfaces and, combining multiple advantages of perovskites with the concept of metasurfaces, we demonstrate that the efficiency of nonlinear multiphoton processes can become comparable to the efficiency of the linear process. We reveal that the perovskite metasurface can enhance substantially two-photon stimulated emission with the threshold being comparable with that of the one-photon process. Our modeling of free-carrier dynamics and exciton recombination upon nonlinear photoexcitation uncovers that this effect can be attributed to the local field enhancement in structured media, a substantial increase of the mode overlap, and the selection rules of two-photon absorption in perovskites.

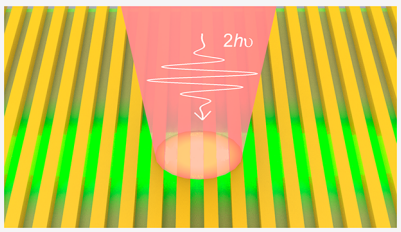

KEYWORDS: *multiphoton absorption, light−matter interaction, grating resonance, local field enhancement*

The study of multiphoton absorption and luminescence from thin films has gained considerable attention during recent years owing to their importance in enriching the fundamental understanding of electronic, vibrational, and rotational states of various materials. In the past decades, several multiphoton processes have been observed and employed for applications such as optical storage,[1−3] stimulated scattering,[4,5] microscopy,[6−8] and nanofabrication.[9,10] Despite a rapid progress in this research direction, wider applications of multiphoton processes in optics are strongly limited because of their overall low efficiencies. As an example, two-photon absorption, being the third-order nonlinear process, requires an excitation power of 2−3 orders of magnitude higher than that required for linear absorption.[11] Recently, several approaches have been developed to enhance the multiphoton light−matter interaction, e.g., by employing plasmonic hot spots with resonances or by using higher-order excitonic states. The enhancement factor of 10^5 has even been demonstrated in experiments.[12] Nevertheless, the overall performance of multiphoton effects usually falls into the category of a weak signal approximation where the power law follows the number of photons involved in the corresponding multiphoton process. More importantly, the required pumping density is far above its linear counterpart in most of the nanostructures, thus significantly hindering the development of many applications of multiphoton nonlinear nanophotonics. An open question is whether any nonlinear multiphoton process can become comparable to or even exceed the linear process for a given material.

RESULTS AND DISCUSSION

To address the above challenges, we aim to improve the system from two aspects. First, a resonant nanostructure should be optimized to enhance the local fields and mode overlapping. Second, we should select materials with extraordinary nonlinear responses. Over the past few years, many types of nonlinear materials have been developed.[3,13,14] Solution-processable lead halide perovskites ($MAPbX_3$, X = Cl, Br, I, and their mixtures) have shown their clear advantages.[4,15−26] A high value of the refractive index ensures strong light confinement, whereas the exceptional nonlinear susceptibility is essential for nonlinear processes including third-harmonic generation and multiphoton stimulated emissions.[16,27,28] Here, by combining the intrinsic advantages of perovskites[23,27,29] with the concept of metamaterials,[17,18,25,30−34] we observe a giant enhancement of two-photon emission from $MAPbBr_3$ perovskite metasurfaces comparable with the one-photon processes.

Figure 1a shows schematically our perovskite metasurface. It consists of a polymer grating on an 80 nm perovskite film. The lattice spacing filling factor and thickness of the grating are l = 395 nm, FF = 0.5, and h = 200 nm, respectively. All structural parameters employed for this work are summarized in Table

Received: May 26, 2021
Revised: August 15, 2021
Published: August 24, 2021

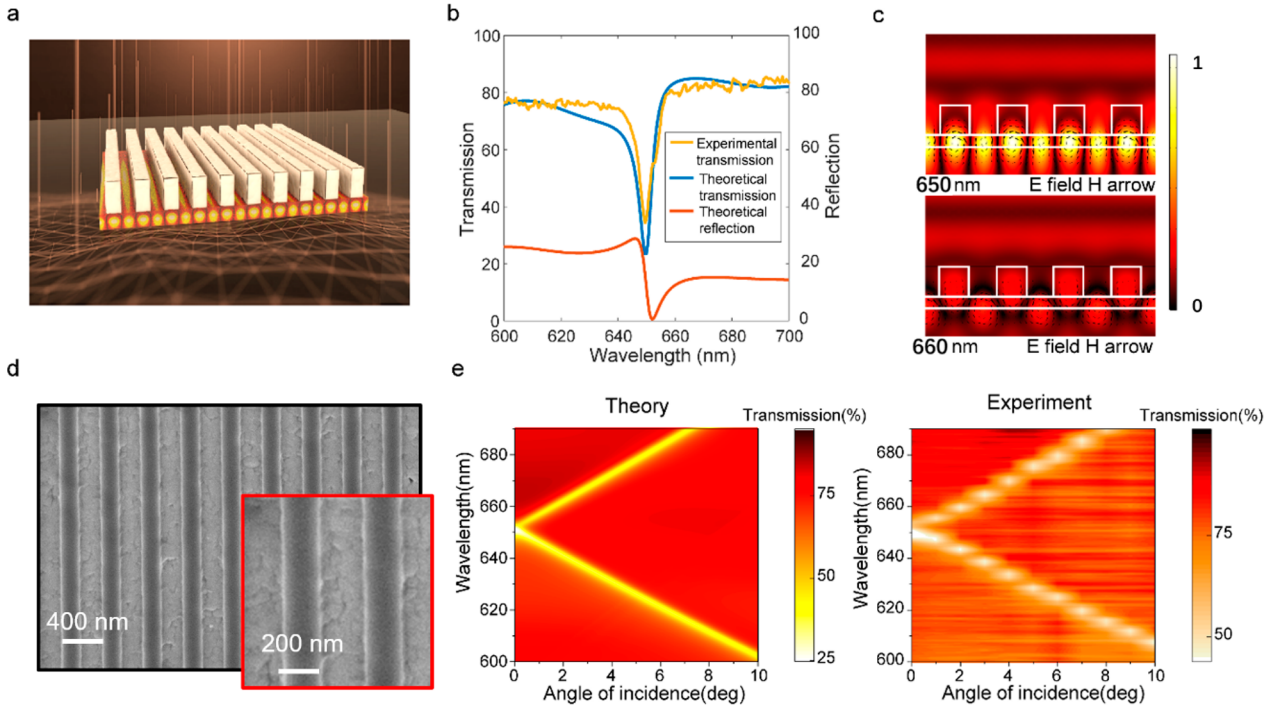

Figure 1. Design of perovskite metasurfaces. (a) Scheme of the perovskite metasurface. (b) Numerically calculated transmission and reflection spectrum at normal incidence and the experimentally recorded transmission spectrum at normal incidence. (c) Vertical cross sections of electromagnetic field distributions at 650 nm (top) and 660 nm (bottom), respectively. (d) Top-view SEM images of the fabricated metasurfaces. (e) Angular dependent transmission spectrum of the perovskite metasurface: theoretical (right) and experimental (left).

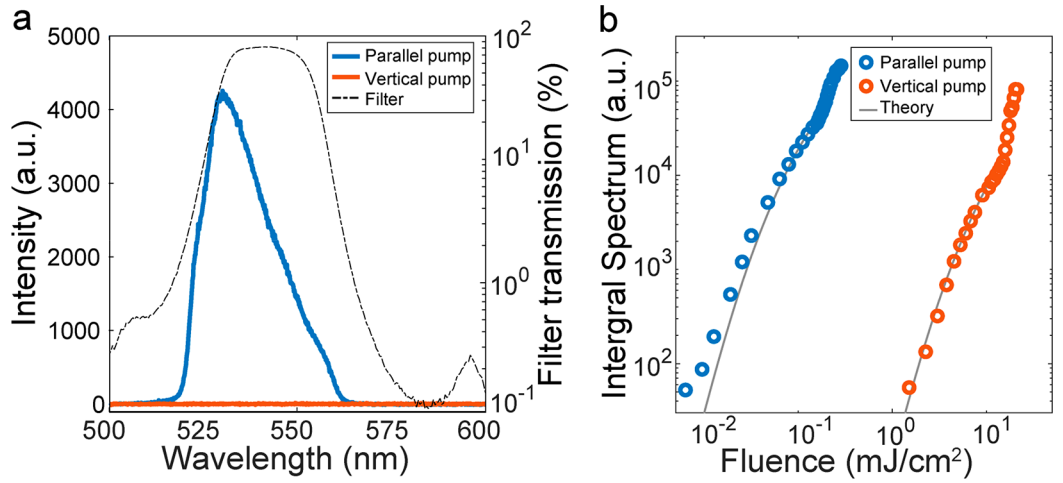

Figure 2. Two-photon photoluminescence in perovskite metasurfaces. (a) Emission spectra from the perovskite metasurface that exited by the parallel pump (solid blue line) and vertical pump (solid red line). Here the pump density is fixed at 0.135 mJ/cm^2. The dashed dotted line shows the transmission spectrum of the filter. (b) Output intensities of two-photon emission that exited by the parallel pump (blue circles) and vertical pump (red circles) as a function of pump fluence. The solid gray curve represents the result of modeling.

S1. In principle, the incident light can be partially coupled into the waveguide mode within the perovskite film via the diffraction of top nanostructures. For a designed incident angle and wavelength, the uncoupled light can destructively interfere with the reradiated waves from the waveguide. Consequently, the transmission can be greatly suppressed, and the incident light is efficiently coupled to the waveguide modes. Figure 1b depicts the numerically calculated transmission (blue curve) and reflection (red curve) spectra at normal incidence. A resonant dip can be clearly seen at 650 nm, where the corresponding reflection is very low. Two panels in Figure 1c show the vertical cross sections of the electric field at the resonant wavelength and 660 nm, respectively. From the direct comparison in Figure 1c and the spectra in Figure 1b it is easy to determine that near 70% of the incident light at the resonant wavelength has been coupled into the waveguide, leading to the strong in-plane confinement and local field enhancement.

In the perovskite metasurface, the intensity of the incident light has been enhanced by 7.7 times (see Figure S1). More importantly, the propagation distance of the waveguide mode can be orders of magnitude longer than the device thickness. Consequently, associated with its exceptional nonlinearity, the proposed perovskite metasurface should be ideal for studying

https://doi.org/10.1021/acs.nanolett.1c02074
Nano Lett. 2021, 21, 7191−7197

the multiphoton processes, and dramatic enhancement can be expected from it. Note that the enhancement is not limited to the angle or wavelength. As depicted in the left part of Figure 1e, the transmission dip splits into two resonances at larger incident angle because of the linear dispersion relation of one-dimension photonic crystal and two mode interaction (see Supporting Information Note 2 and Figure S2), whose confinement and field enhancement are also similar (see Figures S3−S5).

Based on the above analysis, the perovskite metasurface was prepared with spin-coating and patterned with a standard lithographic process (see detail in Supporting Information Note 4). Figure 1d shows the top-view scanning electron microscope (SEM) image of the metasurface. The top polymer grating has straight sidewalls with negligible surface roughness. The lattice size and the filling factor also follow the design. The corresponding angular dependent transmission spectrum of the sample has been characterized with a homemade optical microscope system (see detail in Supporting Information Note 5). The transmission at normal angle is shown in Figure 1b by a yellow line, whereas the angular dependence is presented in the right part of Figure 1e. All the results are consistent with the numerical calculations, clearly demonstrating the promising potential of the fabricated perovskite metasurfaces in multi-photon processes.

Photoluminescence (PL) from the perovskite metasurface was optically excited by weakly focusing a wavelength tunable femtosecond laser onto it (see Figure S6). When the pump laser was tuned to 650 nm with a density of 0.135 mJ/cm^2, a bright green light could be clearly seen with the naked eye. The solid blue line in Figure 2a shows the corresponding emission spectrum, which is a broad photoluminescence peak centered at 530 nm and filtered by a bandpass filter (dash dotted line). The photoluminescence spectrum without using the filter is well consistent with the previous results (see details in Supporting Information Note 6 and Figure S7). This emission spectrum confirms the upconversion process. For a direct comparison, the upconversion photoluminescence of the same perovskite film exited by a vertical pump has also been measured. We notice that the vertical pump and parallel pump mean that the polarization of the pump laser is perpendicular to or parallel to the grating grooves. Under the same pump density, the green emission is very dim and hard to see. The corresponding spectrum (solid red line) in Figure 2a is orders of magnitude weaker, clearly demonstrating the enhancement of two-photon luminescence in the perovskite metasurface. In our design, there is no resonance at the emission wavelength for the vertical case. Consequently, the Purcell effect for spontaneous emission can be neglected, and the main effect can be attributed to the field enhancement and an increase of the propagating length.

Generally, PL in semiconductors is the result of two processes: photoexcitation of charge carriers and light emission via the carrier's recombination. PL power can be represented as $P_{PL}\sim$ QY $\times N_{abs}$, where QY is PL quantum yield and N_{abs} is the number of photoexcited charge carriers. In this regard, the main difference between linear and multiphoton PL is related to the mechanisms of the carrier generation rate. The generation rate for one-photon excitation is $(dN_{abs}/dt)_{1\omega} = \frac{\eta_1}{\tau E_{ph1}}\alpha F$, whereas generation for two-photon excitation is $(dN_{abs}/dt)_{2\omega} = \frac{\eta_2}{\tau^2 E_{ph2}}\beta F^2$, where τ is the pulse duration, E_{ph} is the photon energy, η is the incident light coupling efficiency related to optical resonances in the metasurface, α is the linear absorption coefficient, β is the two-photon absorption coefficient, and F is laser fluence. In turn, QY is determined as the ratio between radiative (R_{rad}) and nonradiative (R_{nr}) recombination rates QY = $R_{rad}/(R_{nr} + R_{rad})$, which can strongly depend on the photogenerated carrier's density.

The dependence of QY on the carrier's density is originated from its fundamental properties. Namely, if the photo-generated carriers form excitons, their radiative recombination rate is a linear function of their density $(R_{rad})_{ex} \sim N_{ex}$. On the other hand, if the binding energy is not enough for stable exciton formation, electrons and holes recombine as free carriers with a radiative recombination rate proportional to the quadratic function of their excess $(R_{rad})_{fc} \sim N_{fc}^2$. Considering the quadratic dependence of the two-photon generation rate on the incident laser fluence, one can derive laws for the PL power for excitons $P_{PL} \sim F^2$ and for free carriers $P_{PL} \sim F^4$. In perovskite $MAPbBr_3$, the binding energy of the bulk exciton is around 40 meV[35] which means that at room temperature 5% of carriers form excitons according to the Saha−Langmuir equation at low fluences. However, the excitonic fraction gradually decreases with an increase of the carrier density (i.e., with an increase of the laser fluence) until the critical density corresponding to the Mott transition, where all carriers become free. This results in the mixing of two types of carriers, and, thus, the dependences of P_{PL} on laser fluence shows a transition from free-carrier-like behavior to the excitonic one. All details and calculations are given in the Supporting Information (see details in Supporting Information Note 7, Table S2, and Figure S8).

The above analysis has been experimentally confirmed by exploring the output intensity as a function of the pumping fluence. Here the coupling efficiency into the metasurface has also been considered for accurate analysis (see Figure S9). The experimental results are summarized as blue circles in Figure 2b. The integrated intensity of PL follows the solid gray line which represents the calculated dependence. Estimation of the slope reveals that it gradually changes from 3.7 at low fluences to a slope of 2 at higher fluences (see details in Supporting Information Note 7). Due to the presence of bimolecular emission, the linear spontaneous emission usually has a slope of 2.0 but can close to 1 due to the contribution of excitons to free carriers.

The red circles in Figure 2b show the reference spectral intensity recorded under the excitation of a 650 nm fs laser polarized vertical to the grating strips (see Figure S10). Since there is no resonance at 650 nm for such a polarization, the local field enhancement and the coupling to the waveguide mode is negligible. As a result, the required fluence is about 2 orders of magnitude higher even though its power-dependent slopes are quite similar. Due to the change in slopes, the enhancement factor is also power dependent. At low fluence, the estimated value is as large as 10^6 (see details in Supporting Information Note 10 and Figure S11).

Based on the dramatic enhancement of two-photon luminescence, it is intriguing to explore whether the multi-photon emission can be comparable to its linear counterpart. To answer this question, we have excited the perovskite metasurface with the femtosecond laser at 400 nm and recorded the emission spectra (see Figure S12). Parts of the results are shown as red lines in Figure 3a. The solid lines of

https://doi.org/10.1021/acs.nanolett.1c02074
Nano Lett. 2021, 21, 7191−7197

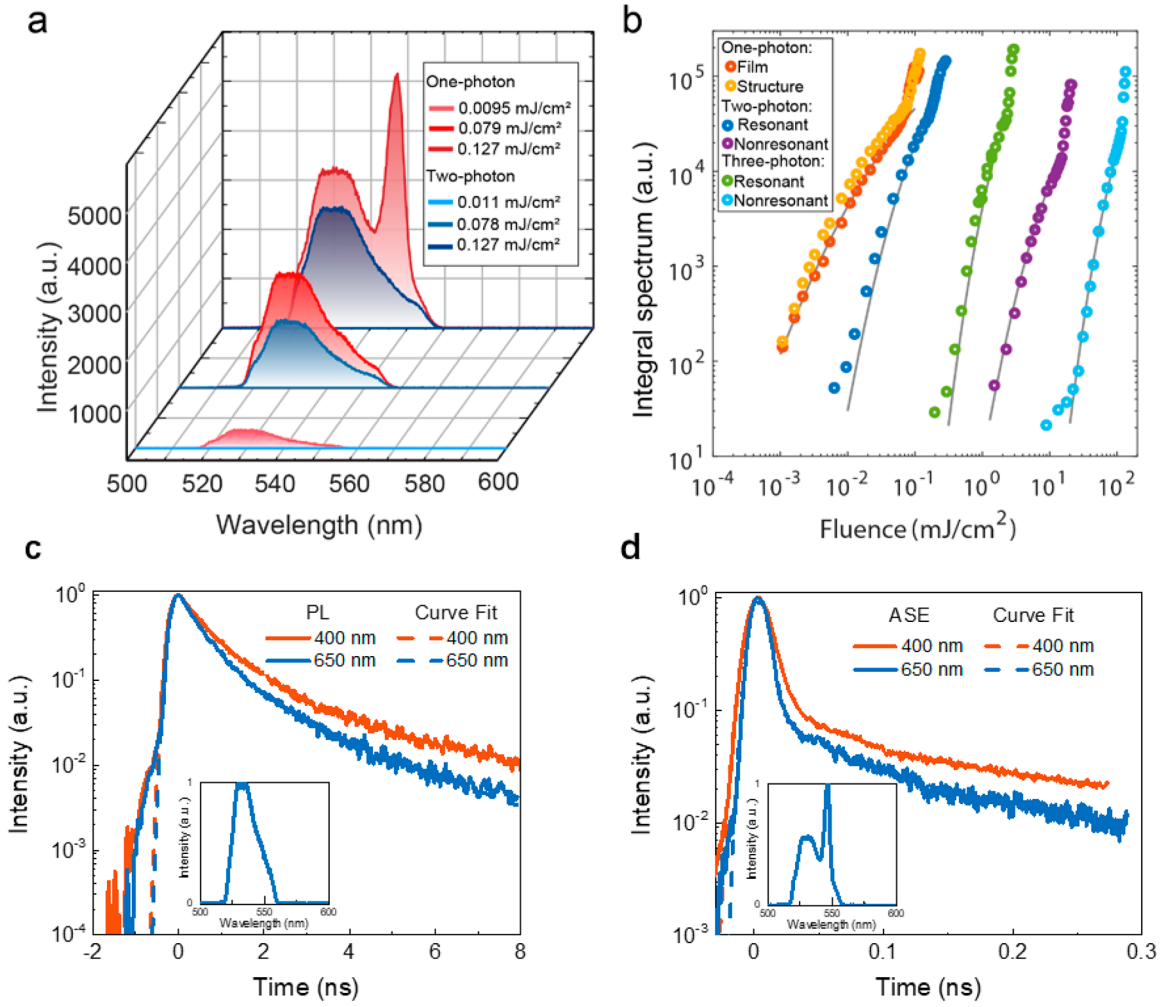

Figure 3. Comparison between one-photon and two-photon emissions. (a) Emission spectra under one-photon and two-photon excitation at three pump fluences. (b) Dependence of integrated intensities under three types of excitations on the pump fluence. The solid gray curves are the results of modeling. (c, d) Time-resolved integrated intensity of photoluminescence under one-photon (red solid line) and two-photon (blue solid line) excitations below and above threshold at 15 K, respectively. Red and blue dashed curves present the corresponding numerical fittings.

blue tint correspond to the two-photon emission recorded with the same pump fluences. When the pumping density is around 10 μJ/cm^2, the intensity of the two-photon emission is about 1/60 of the linear one. Due to the larger slopes of the nonlinear process, the intensity of the two-photon emission increases much faster and is around 60% of the linear emission at a pump fluence of 79 μJ/cm^2. Upon further increase of the pumping fluence, both the linear excitation and the two-photon pumping produce similar spontaneous emissions. The linear excitation reaches the threshold of stimulated emission first, and the two-photon excitation also produces the stimulated emission quickly (see Supporting Information Note 12). The power dependences of one-photon and two-photon emissions are summarized in Figure 3b. It is easy to see that the thresholds for stimulated emission are very close in two cases, indicating the nearly ideal enhancement of multiphoton emission. In the same time, the nonlinear process excites a much lower concentration of full charge carriers than one photon excitation without metasurfaces. Under 0.18 mJ/cm^2 excitation, the concentration of full charge carriers for one-photon excitation N_1 is 4.3 × 10^{19} cm^{-3}. The value for the nonresonant two-photon excitation is N_2 = 9.1 × 10^{14} cm^{-3}, which is far below the linear case. Once the resonance is considered, the value of the two-photon case becomes N_2 = 6.2 × 10^{18} cm^{-3}, comparable to the value of N_1 under one-photon excitation. The details are given in Supporting Information Note 7.

The experimental results shown in Figure 3a,b contradict the common belief that a nonlinear process in a thin nanostructure is much weaker than the corresponding linear process. In general, there are several key parameters that determine the photoluminescence, e.g., the enhancement of excitation, the spontaneous emission coupling factor, the overlapping between stimulated emission and excitation, etc. In our perovskite metasurface, the field enhancement (~7.7 times) at two-photon excitation is confirmed from the simulation of electric field distribution. From our modeling of experimental dependences of PL on pump fluence, we revel that this value of local electric field enhancement equals ~10 for a two-photon resonant parallel pump compared with a vertical pump. Meanwhile, as no resonance appears at the emission wavelength, the spontaneous emission coupling factor of one-photon and two-photon excitation should be the same. The third factor is typically considered to play an essential role in thick crystals and neglected in thin film. Here, however, the situation is different. The 400 nm pumping laser only

https://doi.org/10.1021/acs.nanolett.1c02074
Nano Lett. 2021, 21, 7191−7197

experiences a single pass transmission. In the case of two-photon emission, the resonance at 650 nm can efficiently couple the incident laser into the waveguide mode, transiting the absorption length from thickness to the propagating length along the waveguide. Such a difference makes the overlapping between stimulated emission and excitation in two cases different and induces the two-photon emission approaching the one-photon luminescence.

In addition, the intrinsic material properties of perovskite can also affect the results. Except for a few new materials, the lowest-energy sublevel of bulk halide perovskites is usually dark, and its transition to the ground state is dipole forbidden, if quantum confinement does not affect excitonic properties.[19,20] The emission from such a sublevel requires the assistance of the photon and is typically slow (i.e., order of nanoseconds even at low temperatures). Consequently, this kind of emission cannot attribute to the stimulated emission. On the other hand, the two-photon excitation was widely used to excite such dipole-forbidden PL and, thus, can utilize such transitions and produce higher gain.[36] This conjecture was confirmed experimentally with the time-resolved two-photon luminescence at 15 K (see Figure 3c). One-photon PL has a stronger slow component than the two-photon one. There is a fast time of 0.46 ns and slow time of 1.76 ns for the two-photon pump, whereas for the one-photon pump the times equal 0.58 and 2.48 ns, respectively. The larger slow component under one-photon excitation is preserved at a higher pump fluence. As depicted in Figure 3d, there is still a long tail following the one-photon stimulated emission: the fast time is 0.012 ns and the slow time is 0.34 ns. On the contrary, the two-photon emission rapidly reduces to the noise level ($\sim 10^{-2}$) with fast time of 0.008 ns and slow time of 0.18 ns (Figure 3d). This clearly demonstrates that the one-photon excitation contributes less gain to the system and is consistent with our experimental results. We notice that the resonance with the excitonic states has not been utilized in this experiment. If the higher-energy conduction band states are employed, the enhancement factor can be further improved.[37,38]

It is also important to note that the enhancement in the perovskite metasurface is not limited in the two-photon process. It also holds true for the other nonlinear processes. As shown in Figure 3b, the intensity of the three-photon luminescence is also comparable to the linear fluorescence. The threshold for the three-photon stimulated emission is only 30 times the linear stimulated emission (see Table S3 for multiphoton summary threshold). However, as illustrated in the Figure S14, we must point out here that the enhancements for a four-photon case also happens but is not as significant as for the two- and three-photon cases. This is caused by the competition with THG processes. We can also improve the enhancement factor or decrease the full wave half-maximum (fwhm) by decreasing the refractive index contrast between the environment and polymer grating (see Supporting Information Note 14).

In summary, we have studied experimentally the multiphoton processes in perovskite metasurfaces. We have revealed that two-photon fluorescence in such structures can be enhanced dramatically to become comparable to its linear counterpart. The threshold of two-photon stimulated emission is only 2.7 times the linear one. This effect has been attributed to the local-field enhancement in metasurfaces, a significant increase of an overlap between stimulated emission and excitation modes, and the selection rules in lead-halide perovskites. Similar enhancement has also been observed for three-photon luminescence. Since the main physical mechanism is the field enhancement and increase of the interaction distance, the demonstrated effect should also be observed in other metasurfaces and other materials with high values of the refractive index, e.g., ZnO, GaN, etc. We believe this finding will help to expand applications of multiphoton processes and techniques.

METHODS

Numerical Simulations. All numerical simulations are carried out by using the commercial software COMSOL Multiphysics based on the finite element method. For the design of metasurface, we use a two-dimensional simulation as grating is infinite in the out-of-plane direction; Floquet periodic boundary conditions in the x direction of the unit are employed. The perfectly matched layers (PMLs) are placed on the top and the bottom boundaries to minimize the reflection. The maximum mesh size is 1/10 of the minimum wavelength. Optical properties of all materials used in the simulation are obtained from ellipsometry measurements. A periodic plane-wave with E_z component is excited into the structure along the y direction. We use Particle Swarm Optimization (PSO) to find the best structure parameters that support the strongest enhancement factor. We select five wavelengths around the target resonance wavelength and sum the enhancement factor as a figure of merit (FOM) to smooth the target solution space. We use 20 particles and select parameters of the top ten FOM, to confirm that the enhancement factor has approached the maximum while tolerating the fabrication error.

Deposition of the Perovskite Film. Our metasurface is composed of a 200 nm polymer grating and 80 nm perovskite film for two-photon emission. For the 80 nm $MAPbBr_3$ film, 0.6 mol L^{-1} $MAPbBr_3$ precursor synthesized by dissolving $PbBr_2$ and CH_3NH_3Br powders in dimethyl sulfoxide (DMF) was stirred for 6 h at 80 °C. A total of 50 μL of precursors were then spin-coated onto a 13 nm ITO glass at 4000 r.p.m for 60 s. A total of 70 μL of chlorobenzene was quickly dropped to form an 80 nm dense film during the spin-coating process and then annealed at 100 °C for 10 min. All the above processes were operated in the Ar_2-filled glovebox. The film thickness is accurately controlled by solution concentration and spin speed (see Supporting Information Note 15).

Fabrication of Nanostructures. The polymer grating was fabricated by standard lithographic processes. The 200 nm photoresist (ZEP520 A) was coated on the $MAPbBr_3$ perovskite film, which was patterned by electron beam lithography (Raith Eline 150Plus). The whole size of the sample is 100 × 100 μm^2 with quite good uniformity (see Supporting Information Note 15). The pattern was developed in the developer solution (N50) at room temperature for 50 s after the electron beam irradiation.

Optical Characterization. For the angular dependent transmission spectrum measurement, through adjusting the angle of the 3D-rotate sample stage, the corresponding angular dependent transmission spectrum was coupled to a spectrometer.

For multiphoton photoluminescence measurement, a regenerative amplified femtosecond laser (Spectra-Physics, 800 nm, repetition rate 1 kHz, pulse width 100 fs, seeded by MaiTai) pumped an oscillating parametric amplifier (TOPAS,

https://doi.org/10.1021/acs.nanolett.1c02074
Nano Lett. 2021, 21, 7191−7197

wavelength range: 290 nm−2600 nm) to generate a tunable laser or generate 400 nm second harmonic generation (SHG) from an α-BBO as the pump laser. The pump laser went through a telescope, which consisted of a 75 mm plane-concave lens and a −50 mm plane-concave lens. Changing the distance between the two lenses could adjust the divergence angle of the laser and, thus, change the size of the light spot on the sample. We use the second-moment beam width method to measure beam diameter from a picture.

■ ASSOCIATED CONTENT

Supporting Information

The Supporting Information is available free of charge at https://pubs.acs.org/doi/10.1021/acs.nanolett.1c02074.

Description of the optical properties of the metasurface for numerical simulations, mode interaction between two resonances, confinement and field enhancement under a large incident angle, sample fabrication, optical characterization measurement, photoluminescence spectrum influenced by the bandpass filter, modeling of fluence dependences, coupling efficiency into the metasurface, polarization selected resonance, emission enhancement at low fluence, emission spectra excited by one photon, two-photon amplified spontaneous emission (ASE) spectrum, multiphoton enhancement comparison, improve enhancement factor and decreased fwhm, and uniformity of the sample and accurate control of the thickness of the film (PDF)

■ AUTHOR INFORMATION

Corresponding Authors

Shumin Xiao − *Ministry of Industry and Information Technology Key Lab of Micro-Nano Optoelectronic Information System, Shenzhen Graduate School, Harbin Institute of Technology Shenzhen, Shenzhen 518055, P. R. China; National Key Laboratory of Science and Technology on Advanced Composites in Special Environments, Harbin Institute of Technology, Harbin 150080, P. R. China; Collaborative Innovation Center of Extreme Optics, Shanxi University, Taiyuan 030006 Shanxi, P. R. China*; Email: shumin.xiao@hit.edu.cn

Yuri Kivshar − *ITMO University, St. Petersburg 197101, Russia; Nonlinear Physics Center, Research School of Physics, Australian National University, Canberra, Australian Capital Territory 2601, Australia*; orcid.org/0000-0002-3410-812X; Email: yuri.kivshar@anu.edu.au

Sergey V. Makarov − *ITMO University, St. Petersburg 197101, Russia*; orcid.org/0000-0002-9257-6183; Email: makarov_sergey_vl@mail.ru

Qinghai Song − *Ministry of Industry and Information Technology Key Lab of Micro-Nano Optoelectronic Information System, Shenzhen Graduate School, Harbin Institute of Technology Shenzhen, Shenzhen 518055, P. R. China*; orcid.org/0000-0003-1048-411X; Email: qinghai.song@hit.edu.cn

Authors

Yubin Fan − *Ministry of Industry and Information Technology Key Lab of Micro-Nano Optoelectronic Information System, Shenzhen Graduate School, Harbin Institute of Technology Shenzhen, Shenzhen 518055, P. R. China*

Pavel Tonkaev − *ITMO University, St. Petersburg 197101, Russia; Nonlinear Physics Center, Research School of Physics, Australian National University, Canberra, Australian Capital Territory 2601, Australia*

Yuhan Wang − *Ministry of Industry and Information Technology Key Lab of Micro-Nano Optoelectronic Information System, Shenzhen Graduate School, Harbin Institute of Technology Shenzhen, Shenzhen 518055, P. R. China*

Jiecai Han − *National Key Laboratory of Science and Technology on Advanced Composites in Special Environments, Harbin Institute of Technology, Harbin 150080, P. R. China*

Complete contact information is available at: https://pubs.acs.org/10.1021/acs.nanolett.1c02074

Author Contributions

#(Y.F, P.T., and Y.W.) These authors contributed equally to this work.

Notes

The authors declare no competing financial interest.

■ ACKNOWLEDGMENTS

Q.S. and S.X. acknowledge financial support from the National Natural Science Foundation of China (Grants 11974092, 12025402, 61975041, and 11934012), National Key Research and Development Program of China (Grant SQ2018YFB220027), Fundamental Research Funds for the Central Universities, and Shenzhen Fundamental Research Projects (Grants JCYJ20180507183532343, JCYJ20180507184613841, and JCYJ20180306172041577). This work was partially supported by the Ministry of Science and Higher Education of the Russian Federation (Project 075-15-2021-589) and the Australian Research Council (Grants DP200101168 and DP210101292).

■ REFERENCES

(1) Lott, J.; Ryan, C.; Valle, B.; Johnson, J. R.; Schiraldi, D. A.; Shan, J.; Singer, K. D.; Weder, C. Two-Photon 3D Optical Data Storage via Aggregate Switching of Excimer-Forming Dyes. *Adv. Mater.* **2011**, *23*, 2425−2429.

(2) Olson, C. E.; Previte, M. J. R.; Fourkas, J. T. Efficient and Robust Multiphoton Data Storage in Molecular Glasses and Highly Crosslinked Polymers. *Nat. Mater.* **2002**, *1*, 225−228.

(3) Liu, X.; Jia, X.; Fischer, M.; Huang, Z.; Smith, D. R. Enhanced Two-Photon Photochromism in Metasurface Perfect Absorbers. *Nano Lett.* **2018**, *18*, 6181−6187.

(4) He, G. S.; Chen, K.; Liu, J.; Prasad, P. N. Two-Photon Excitation Enhanced High-Efficiency and Phase-Conjugate Stimulated Mie Scattering of Perovskite Nanocrystals Suspended in n-Hexane. *J. Phys. Chem. C* **2020**, *124*, 25944−25950.

(5) Traverso, A. J.; Hokr, B.; Yi, Z.; Yuan, L.; Yamaguchi, S.; Scully, M. O.; Yakovlev, V. V. Two-Photon Infrared Resonance Can Enhance Coherent Raman Scattering. *Phys. Rev. Lett.* **2018**, *120*, 063602.

(6) Arbabi, E.; Li, J.; Hutchins, R. J.; Kamali, S. M.; Arbabi, A.; Horie, Y.; Van Dorpe, P.; Gradinaru, V.; Wagenaar, D. A.; Faraon, A. Two-Photon Microscopy with a Double-Wavelength Metasurface Objective Lens. *Nano Lett.* **2018**, *18*, 4943−4948.

(7) Stavrakas, C.; Delport, G.; Zhumekenov, A. A.; Anaya, M.; Chahbazian, R.; Bakr, O. M.; Barnard, E. S.; Stranks, S. D. Visualizing Buried Local Carrier Diffusion in Halide Perovskite Crystals via Two-Photon Microscopy. *ACS Energy Lett.* **2020**, *5*, 117−123.

(8) Li, B.; Wu, C.; Wang, M.; Charan, K.; Xu, C. An Adaptive Excitation Source for High-Speed Multiphoton Microscopy. *Nat. Methods* **2020**, *17*, 163−166.

(9) Geng, Q.; Wang, D.; Chen, P.; Chen, S.-C. Ultrafast Multi-Focus 3-D Nano-Fabrication Based on Two-Photon Polymerization. *Nat. Commun.* **2019**, *10*, 2179.
(10) Zhou, C.; Cao, G.; Gan, Z.; Ou, Q.; Chen, W.; Bao, Q.; Jia, B.; Wen, X. Spatially Modulating the Fluorescence Color of Mixed-Halide Perovskite Nanoplatelets through Direct Femtosecond Laser Writing. *ACS Appl. Mater. Interfaces* **2019**, *11*, 26017−26023.
(11) Soria, S.; N., A. T. K.; Badenes, G.; Bader, M. A.; Selle, A.; Marowsky, G. Resonant Double Grating Waveguide Structures as Enhancement Platforms for Two-Photon Fluorescence Excitation. *Appl. Phys. Lett.* **2005**, *87*, 081109.
(12) Flauraud, V.; Regmi, R.; Winkler, P. M.; Alexander, D. T. L.; Rigneault, H.; van Hulst, N. F.; García-Parajo, M. F.; Wenger, J.; Brugger, J. In-Plane Plasmonic Antenna Arrays with Surface Nanogaps for Giant Fluorescence Enhancement. *Nano Lett.* **2017**, *17*, 1703−1710.
(13) Nevet, A.; Berkovitch, N.; Hayat, A.; Ginzburg, P.; Ginzach, S.; Sorias, O.; Orenstein, M. Plasmonic Nanoantennas for Broad-Band Enhancement of Two-Photon Emission from Semiconductors. *Nano Lett.* **2010**, *10*, 1848−1852.
(14) Semmlinger, M.; Tseng, M. L.; Yang, J.; Zhang, M.; Zhang, C.; Tsai, W. Y.; Tsai, D. P.; Nordlander, P.; Halas, N. J. Vacuum Ultraviolet Light-Generating Metasurface. *Nano Lett.* **2018**, *18*, 5738−5743.
(15) Saba, M.; Cadelano, M.; Marongiu, D.; Chen, F.; Sarritzu, V.; Sestu, N.; Figus, C.; Aresti, M.; Piras, R.; Geddo Lehmann, A.; Cannas, C.; Musinu, A.; Quochi, F.; Mura, A.; Bongiovanni, G. Correlated Electron−Hole Plasma in Organometal Perovskites. *Nat. Commun.* **2014**, *5*, 5049.
(16) Gao, Y.; Wang, S.; Huang, C.; Yi, N.; Wang, K.; Xiao, S.; Song, Q. Room Temperature Three-Photon Pumped $CH_3NH_3PbBr_3$ Perovskite Microlasers. *Sci. Rep.* **2017**, *7*, 45391.
(17) Makarov, S. V.; Milichko, V.; Ushakova, E. V.; Omelyanovich, M.; Cerdan Pasaran, A.; Haroldson, R.; Balachandran, B.; Wang, H.; Hu, W.; Kivshar, Y. S.; Zakhidov, A. A. Multifold Emission Enhancement in Nanoimprinted Hybrid Perovskite Metasurfaces. *ACS Photonics* **2017**, *4*, 728−735.
(18) Becker, C.; Burger, S.; Barth, C.; Manley, P.; Jäger, K.; Eisenhauer, D.; Köppel, G.; Chabera, P.; Chen, J.; Zheng, K.; Pullerits, T. Nanophotonic-Enhanced Two-Photon-Excited Photoluminescence of Perovskite Quantum Dots. *ACS Photonics* **2018**, *5*, 4668−4676.
(19) Becker, M. A.; Vaxenburg, R.; Nedelcu, G.; Sercel, P. C.; Shabaev, A.; Mehl, M. J.; Michopoulos, J. G.; Lambrakos, S. G.; Bernstein, N.; Lyons, J. L.; Stöferle, T.; Mahrt, R. F.; Kovalenko, M. V.; Norris, D. J.; Rainò, G.; Efros, A. L. Bright Triplet Excitons in Caesium Lead Halide Perovskites. *Nature* **2018**, *553*, 189−193.
(20) Chen, L.; Li, B.; Zhang, C.; Huang, X.; Wang, X.; Xiao, M. Composition-Dependent Energy Splitting between Bright and Dark Excitons in Lead Halide Perovskite Nanocrystals. *Nano Lett.* **2018**, *18*, 2074−2080.
(21) Saouma, F. O.; Stoumpos, C. C.; Kanatzidis, M. G.; Kim, Y. S.; Jang, J. I. Multiphoton Absorption Order of $CsPbBr_3$ as Determined by Wavelength-Dependent Nonlinear Optical Spectroscopy. *J. Phys. Chem. Lett.* **2017**, *8*, 4912−4917.
(22) Grinblat, G.; Abdelwahab, I.; Nielsen, M. P.; Dichtl, P.; Leng, K.; Oulton, R. F.; Loh, K. P.; Maier, S. A. Ultrafast All-Optical Modulation in 2D Hybrid Perovskites. *ACS Nano* **2019**, *13*, 9504−9510.
(23) Kriso, C.; Stein, M.; Haeger, T.; Pourdavoud, N.; Gerhard, M.; Rahimi-Iman, A.; Riedl, T.; Koch, M. Nonlinear Refraction in $CH_3NH_3PbBr_3$ Single Crystals. *Opt. Lett.* **2020**, *45*, 2431−2434.
(24) Li, J.; Jing, Q.; Xiao, S.; Gao, Y.; Wang, Y.; Zhang, W.; Sun, X. W.; Wang, K.; He, T. Spectral Dynamics and Multiphoton Absorption Properties of All-Inorganic Perovskite Nanorods. *J. Phys. Chem. Lett.* **2020**, *11*, 4817−4825.
(25) Zhou, Y.; Huang, Y.; Xu, X.; Fan, Z.; Khurgin, J. B.; Xiong, Q. Nonlinear Optical Properties of Halide Perovskites and Their Applications. *Appl. Phys. Rev.* **2020**, *7*, 041313.
(26) Hu, Z. P.; Liu, Z. Z.; Zhan, Z. J.; Shi, T. C.; Du, J.; Tang, X. S.; Leng, Y. X. Advances in metal halide perovskite lasers: synthetic strategies, morphology control, and lasing emission. *Adv. Photonics* **2021**, *3*, 034002.
(27) Fan, Y.; Wang, Y.; Zhang, N.; Sun, W.; Gao, Y.; Qiu, C. W.; Song, Q.; Xiao, S. Resonance-Enhanced Three-Photon Luminesce via Lead Halide Perovskite Metasurfaces for Optical Encoding. *Nat. Commun.* **2019**, *10*, 2085.
(28) He, G. S.; Markowicz, P. P.; Lin, T. C.; Prasad, P. N. Observation of Stimulated Emission by Direct Three-Photon Excitation. *Nature* **2002**, *415*, 767−770.
(29) Wei, T. C.; Mokkapati, S.; Li, T. Y.; Lin, C. H.; Lin, G. R.; Jagadish, C.; He, J. H. Nonlinear Absorption Applications of $CH_3NH_3PbBr_3$ Perovskite Crystals. *Adv. Funct. Mater.* **2018**, *28*, 1707175.
(30) Löchner, F. J. F.; Fedotova, A. N.; Liu, S.; Keeler, G. A.; Peake, G. M.; Saravi, S.; Shcherbakov, M. R.; Burger, S.; Fedyanin, A. A.; Brener, I.; Pertsch, T.; Setzpfandt, F.; Staude, I. Polarization-Dependent Second Harmonic Diffraction from Resonant GaAs Metasurfaces. *ACS Photonics* **2018**, *5*, 1786−1793.
(31) Adamo, G.; Swaha Krishnamoorthy, H. N.; Cortecchia, D.; Chaudhary, B.; Nalla, V.; Zheludev, N. I.; Soci, C. Metamaterial Enhancement of Metal-Halide Perovskite Luminescence. *Nano Lett.* **2020**, *20*, 7906−7911.
(32) Quaranta, G.; Basset, G.; Martin, O. J. F.; Gallinet, B. Recent Advances in Resonant Waveguide Gratings. *Laser Photon. Rev.* **2018**, *12*, 1800017.
(33) Liu, S.; Vabishchevich, P. P.; Vaskin, A.; Reno, J. L.; Keeler, G. A.; Sinclair, M. B.; Staude, I.; Brener, I. An All-Dielectric Metasurface as a Broadband Optical Frequency Mixer. *Nat. Commun.* **2018**, *9*, 2507.
(34) Poddubny, A. N.; Ginzburg, P.; Belov, P. A.; Zayats, A. V.; Kivshar, Y. S. Tailoring and Enhancing Spontaneous Two-Photon Emission Using Resonant Plasmonic Nanostructures. *Phys. Rev. A: At., Mol., Opt. Phys.* **2012**, *86*, 033826.
(35) Yang, Y.; Yang, M.; Li, Z.; Crisp, R.; Zhu, K.; Beard, M. C. Comparison of Recombination Dynamics in $CH_3NH_3PbBr_3$ And $CH_3NH_3PbI_3$ Perovskite Films: Influence of Exciton Binding Energy. *J. Phys. Chem. Lett.* **2015**, *6*, 4688−4692.
(36) Hohlneicher, G.; Dick, B. Two-photon Spectroscopy of Dipole-forbidden Transitions. II. Calculation of Two-photon Cross Sections by the CNDO−CI Method. *J. Chem. Phys.* **1979**, *70*, 5427−5437.
(37) Ohara, K.; Yamada, T.; Aharen, T.; Tahara, H.; Hirori, H.; Suzuura, H.; Kanemitsu, Y. Impact of Spin-Orbit Splitting on Two-Photon Absorption Spectra in A Halide Perovskite Single Crystal. *Phys. Rev. B: Condens. Matter Mater. Phys.* **2021**, *103*, L041201.
(38) Yumoto, G.; Hirori, H.; Sekiguchi, F.; Sato, R.; Saruyama, M.; Teranishi, T.; Kanemitsu, Y. Strong Spin-Orbit Coupling Inducing Autler-Townes Effect in Lead Halide Perovskite Nanocrystals. *Nat. Commun.* **2021**, *12*, 3026.

https://doi.org/10.1021/acs.nanolett.1c02074
Nano Lett. 2021, 21, 7191−7197